

UNIVERSITÉ CATHOLIQUE DE LOUVAIN

---

**Study of the stress relieve heat-treatment of  
additively manufactured AlSi10Mg alloy:**  
Influence on microstructure and mechanical properties

---

*Dissertation presented by*

David DISPAS                      *and*                      Arthur BOUILLOT

*for obtaining the Master's degree in*

Mechanical Engineering                      *and*                      Chemical and Materials  
Engineering

*at Ecole Polytechnique de Louvain (EPL)*

*Supervisor:* Aude SIMAR

*Readers:* Laurent DELANNAY, Anne MERTENS, Camille VAN DER REST

Academic year 2017-2018

*'Citation stylée.'*

Mec cool

# Acknowledgements

Blablabla. blabla. bla.



# Contents

<b>1</b>	<b>Introduction</b>	<b>1</b>
<b>2</b>	<b>State of the art</b>	<b>3</b>
<b>3</b>	<b>Materials and methods</b>	<b>9</b>
3.1	Powder follow-up . . . . .	9
3.1.1	Sieving . . . . .	9
3.1.2	Grain size and distribution . . . . .	9
3.1.3	Composition . . . . .	9
3.2	Process parameters . . . . .	9
3.3	Heat treatments . . . . .	10
3.4	Characterisation . . . . .	10
3.4.1	Density . . . . .	10
	Hydrostatic weighing . . . . .	10
	Relative optical density image analysis . . . . .	11
3.4.2	Microscopy . . . . .	12
	Scanning electron microscopy . . . . .	12
	Optical microscopy . . . . .	12
3.4.3	Composition . . . . .	12
3.4.4	Mechanical properties . . . . .	12
	Hardness test . . . . .	12
	Traction test . . . . .	13
<b>4</b>	<b>Results</b>	<b>15</b>
4.1	Parameters optimisation . . . . .	15
4.2	Reproducibility . . . . .	15
4.3	Powder ageing . . . . .	15
4.3.1	Grain size and distribution . . . . .	15
4.3.2	Composition . . . . .	15
	Fresh powder . . . . .	15
	Recycled powder . . . . .	15
4.4	Heat treatments . . . . .	15
4.5	Mechanical testing . . . . .	15
<b>5</b>	<b>Discussion</b>	<b>17</b>
5.1	Parameters optimisation . . . . .	17
5.2	Reproducibility . . . . .	17
5.3	Powder ageing . . . . .	17
5.3.1	Grain size and distribution . . . . .	17
5.3.2	Composition . . . . .	17
5.4	Density measures assessments . . . . .	17
5.5	Heat treatment optimisation . . . . .	17

<b>6 Conclusion</b>	<b>19</b>
<b>A Calculs supplémentaires</b>	<b>21</b>
A.1 ...	21
A.2 ...	21
<b>Bibliography</b>	<b>23</b>

# List of Figures

2.1	Selective laser melting technology principle . . . . .	3
2.2	(a)Research publications on SLM of ceramics, composites and all materials types combined. (b)Research publications on SLM of different metallic materials . . . . .	4
2.3	Parameters involved in SLM . . . . .	5
2.4	Process window for SLM of AlSi10Mg, based on the top view of single track scans . . . . .	6
2.5	Process window for SLM of AlSi10Mg, based on the front view of single track scans . . . . .	6
2.6	Schematic representation of scanning strategies commonly used in LSM (a) unidirectional long scan track; (b) bi-directional long scan track, and (c) islands . . . . .	7
2.7	Samples (static tensile) built in different directions: (a) 0°, (b) 45°, and (c) 90° . . . . .	7
3.1	ProX DMP 200 printer . . . . .	10
3.2	Melt pool contours with and without laser compensation (exaggeration) . . . . .	11
3.3	Laser compensations as a function of the scanning speed (as recommended by the manufacturer) . . . . .	12
3.4	Dimensions notations for (a) cubic specimens (b) cylindrical specimens . . . . .	13
3.5	RODIA procedure for specimen X200-180319-cub 1: (a) Original picture of polished section (b) Whole surface isolation with <i>ImageJ</i> (c) Porosities isolation with <i>ImageJ</i> . . . . .	13





# List of Tables

3.1	Process parameters used for the specimens manufacturing . . . . .	14
3.2	Polishing routine for Al-Si alloys . . . . .	14
4.1	Composition of recycled AlSi10Mg powder as a function of the date .	15



# List of Abbreviations

<b>AM</b>	<b>Additive Manufacturing</b>
<b>CAD</b>	<b>Computer Aided Design</b>
<b>DMLS</b>	<b>Direct Metal Laser Sintering</b>
<b>DMP</b>	<b>Direct Metal Printer</b>
<b>ICP</b>	<b>Inductively Coupled Plasma</b>
<b>RODIA</b>	<b>Relative Optical Density Image Analysis</b>
<b>SEM</b>	<b>Scanning Electron Microscope</b>
<b>SLM</b>	<b>Selective Laser Melting</b>



# Symbols

$D_a$	Average particle size	$[\mu m]$
$E_d$	Volumetric energy density	$[\frac{J}{mm^3}]$
$h$	Hatch space	$[\mu m]$
$H_v$	Vickers hardness	$[HV]$
$P$	Laser power	$[W]$
$p_{O_2}$	Oxygen pressure	$[mbar]$
$t$	Layer thickness	$[\mu m]$
$v_s$	Scanning speed	$[\frac{mm}{s}]$
$W_a$	Specimen dry weight	$[g]$
$W_w$	Specimen underwater weight	$[g]$
$\phi_{99\%}$	Laser spot size at the 99% contour	$[\mu m]$
$\lambda$	Laser wavelength	$[nm]$
$\rho_a$	Apparent density	$[\frac{g}{cm^3}]$
$\rho_{a,rel}$	Apparent relative density	$[-]$
$\rho_w$	Water density	$[\frac{g}{cm^3}]$
$\rho_{rel}$	Relative density	$[-]$



*Nous dédions ce travail à nos familles et amis*





## Chapter 1

# Introduction

This is, with the concluding chapter, a significant portion of memory. This should especially present the context and objectives of the work. Generally, the memory structure (content of chapters) is briefly exposed



## Chapter 2

# State of the art

Selective laser melting (SLM) - also referred to as direct metal laser sintering (DMLS) - is an additive manufacturing (AM) technique making use of a high power-density laser that locally melts powder materials. When a layer of powder has been melted, a new layer is spread on top of the previous one, and is in turn melted, in order to progressively build a 3D object. The technique is illustrated on figure 2.1 [12]. The materials used include mostly metals but also ceramics and composites. Parts to build must first be drawn in a computer-aided design (CAD) software and broken down in 2D slices, each one corresponding to a powder layer. During the process, the oxygen pressure  $p_{O_2}$  must be kept low to prevent the oxidation of the metal. A shielding gas - such as argon - is thus used to fill the build chamber at all time, while  $p_{O_2}$  is monitored.

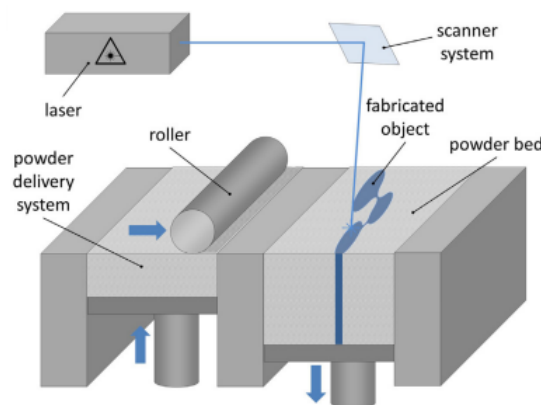


FIGURE 2.1: Selective laser melting technology principle (from Leitz et al, 2016).

LSM is still a young technology. Its popularity only increased significantly over the last decade, as depicted by figures 2.2 (a) and (b). Works concerning AlSi10Mg began to emerge noticeably in 2014. The technique usage spread rapidly in many sectors: biomedical, heat exchangers, aerospace and automotive - to name just a few [23]. This is due to the numerous appeals of SLM compared to the other technologies, including:

- Geometrical flexibility: parts can be designed with thin walls or even with hidden cavities and/or channels. This offers promising prospects regarding light-weight potentials for parts solicited mechanically [13];

- Increased reliability of the parts [8];
- Reduced equipment costs [9];
- Better operational efficiency: the fabrication is quick and easy which reduces time-to-market as well as assembly times and capital tied up in stocks [9];
- Individual production facilitation [8];
- Reduced material waste and better energy usage: the process is environmentally friendly as a whole [8].

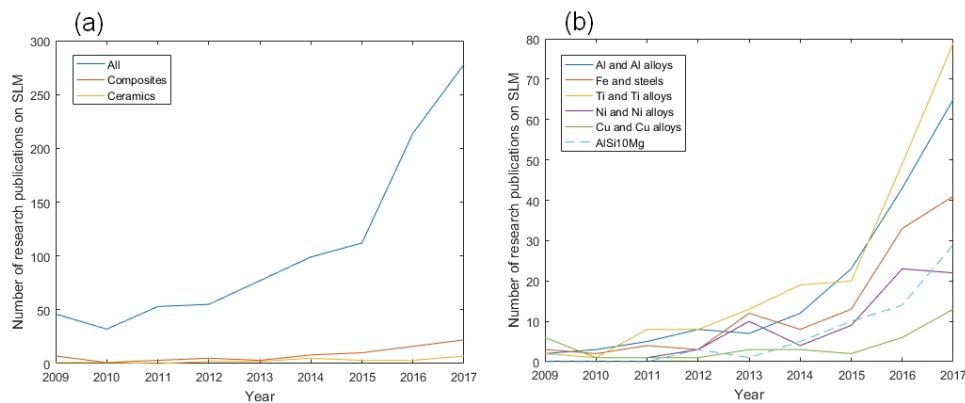


FIGURE 2.2: (a) Research publications on SLM of ceramics, composites and all materials types combined. (b) Research publications on SLM of different metallic materials. Data are derived from the research publications on SLM, LaserCusing and DMLS existing on ScienceDirect website.

Parler de l'AlSi10Mg; quel est l'intérêt de travailler avec? Difficultés? (reflectivité etc)

#### Microstructure homogène, diagramme de phase

The properties of parts produced through SLM stem from the coupled effects of a great deal of parameters (see figure 2.3) [3]. Results are very sensitive to their variations. The process parameters must thus be monitored thoroughly. This complicates the search for their optimisation, still not fully resolved for aluminium alloys.

In recent years, works aiming at facing this challenge multiplied. The minimisation of the porosity is at the center of attention. It is indeed closely related to the quality of the mechanical properties. As porosity contributes to lowering the load-bearing surface, it reduces the apparent material strength. It was also observed to have a critical influence on the fatigue life of the produced parts. Their lifetime is especially diminished if the values of pores amount and size go beyond a certain threshold [5]. Studies investigating the effects of various parameters on the AlSi10Mg fabrication through SLM abound in the literature.

The analysis of the paired impacts of the laser power  $P$  and scan speed  $v_s$  provides a first insight. As depicted by figures 2.4 and 2.5, low  $P$  and high  $v_s$  lead to an insufficient energy input to melt the powder and re-melt the substrate, which causes the formation of droplets [11]. The opposite leads to good penetration but also to

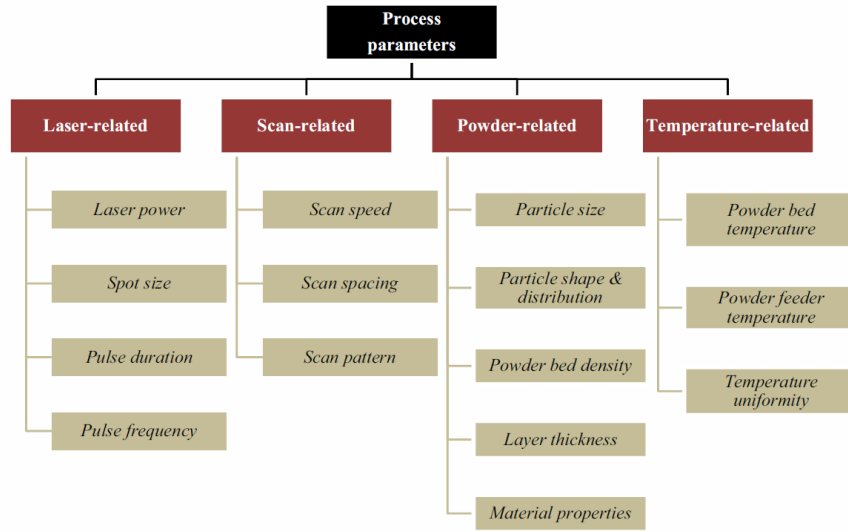


FIGURE 2.3: Parameters involved in SLM (from Aboulkhair et al, 2014).

distortions and irregularities. A trend to use both high  $P$  and  $v_s$  rose in accordance with these findings. Doing so has the advantage to increase productivity. However, it also has multiple downsides including a decrease of the surface quality due to balling, excessive spatter, and an augmented gas induced porosity [15]. Therefore, a trade-off must be found.

A popular approach is to regroup multiple operating parameters into one, the volumetric energy density  $E_d$ . It is estimated through the following formula:

$$E_d = \frac{P}{v_s h t}$$

where  $t$  is the layer thickness and  $h$  is the hatch space. As a rule of thumb,  $E_d$  should be chosen in the range between 60 and 75 [ $\frac{J}{mm^3}$ ] [17]. However, the criterion is insufficient and others phenomena, such as melt pools overlapping, should be considered [20]. Very few studies were carried out to optimize  $h$  and  $t$  independently. Their values lie generally respectively in the intervals [50 ; 200] [ $\mu m$ ] and [20 ; 60] [ $\mu m$ ]. It was observed that for  $t = 30$  [ $\mu m$ ], an optimal set of parameters values in terms of density is  $P = 200$  [W],  $v_s = 1400$  [ $\frac{mm}{s}$ ] and  $h = 105$  [ $\mu m$ ] [11].

The other process parameters will be covered for the sake of completeness. Let us first look into the particle-related parameters. The particle size  $D_a$  of the powder should be as small as possible to ensure a good flowability and allow for thin layers [11]. Typical values stretch from 15 to 60 [ $\mu m$ ]. The size distribution is more delicate to outline. On one hand, wider distributions often generate better bed density, parts with higher density and better surface finish. On the other hand, narrower ones usually provide better flowability and parts with better strength and hardness [14]. In most cases, a middle ground between the two should be sought. In SLM applications, powder is often successively recycled multiple times. This leads to their progressive contamination with moisture, which causes an increase of hydrogen porosity in the produced parts [22]. The problem can be overcome by drying

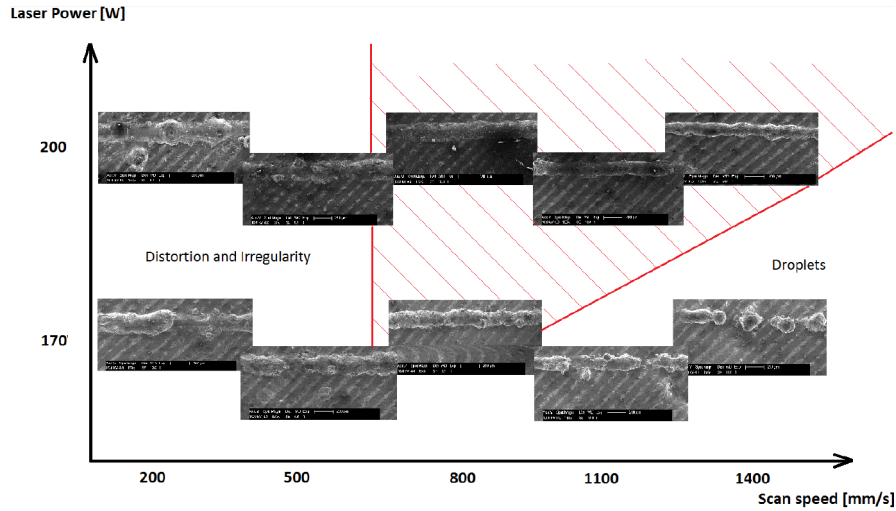


FIGURE 2.4: Process window for SLM of AlSi10Mg, based on the top view of single track scans (from Kempen et al, 2011).

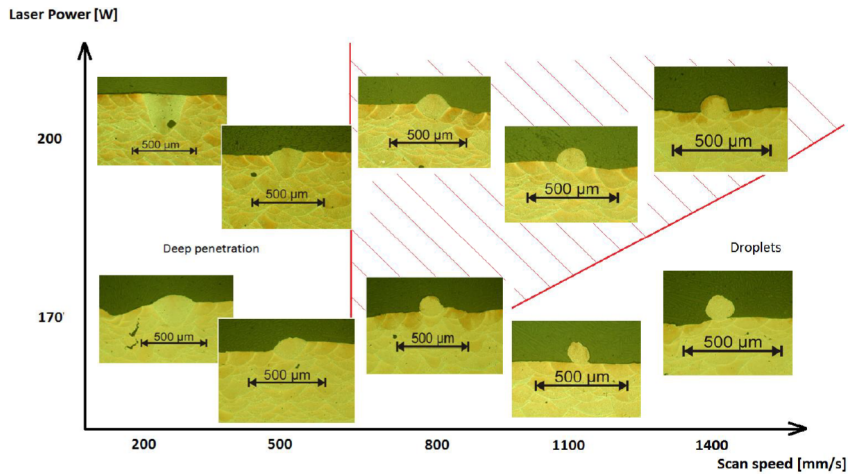


FIGURE 2.5: Process window for SLM of AlSi10Mg, based on the front view of single track scans (from Kempen et al, 2011).

the powder or using fresh one. Unfortunately - in the case of aluminium alloys - no findings were made regarding the prediction of a threshold at which one should take action [4].

The choice of scan pattern has great importance. There exist a few different strategies. The common ones use unidirectional, bidirectional or islands patterns (see figure 2.6). The scan direction(s) should be rotated between successive layers to favorise isotropy, especially in the unidirectional case since it causes height variations along a layer [2]. The islands pattern is based on a decomposition in small domains with short scanning tracks. Two usual strategies can be distinguished among this group: the chessboard and the hexagonal one.

Furthermore, dual scanning strategies were proven to be effective. For example, a pre-scan with low  $E_d$  can flatten the powder bed before it is consolidated, which

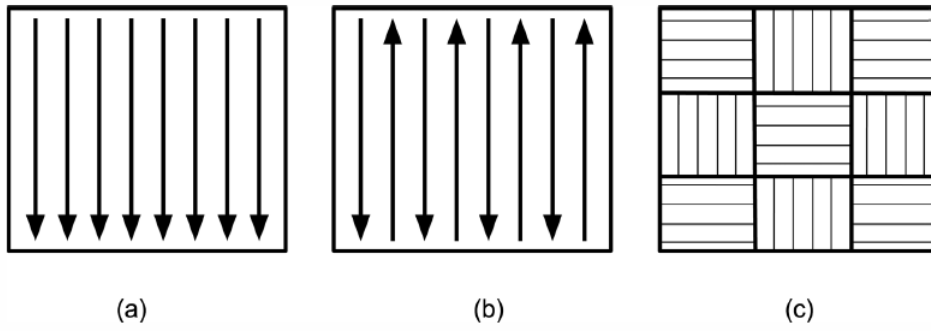


FIGURE 2.6: Schematic representation of scanning strategies commonly used in LSM (a) unidirectional long scan track; (b) bi-directional long scan track, and (c) islands (from Mertens et al, 2017).

leads to a reduction of porosity [15]. It was also shown that scanning the contour of the part being built at lower  $E_d$  can better the surface roughness for AlSi12Mg [16]. One should note too that the final properties of the fabricated part can strongly depend on the building direction (see figure 2.7) [7].

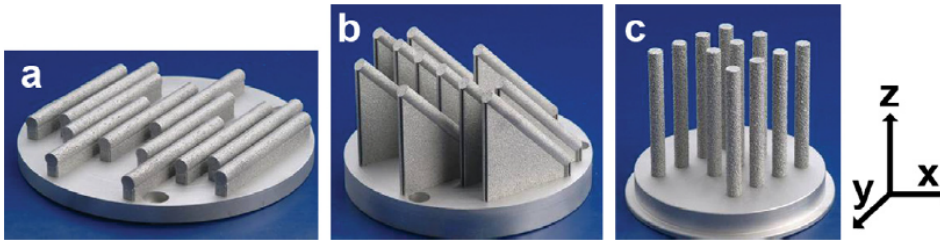


FIGURE 2.7: Samples (static tensile) built in different directions: (a) 0°, (b) 45°, and (c) 90° (from Brandl et al, 2012).

Other laser-related parameters - the spot size and the pulse properties - can also influence the process. Only the laser spot size at the 99% contour  $\phi_{99\%}$  is frequently cited in literature. Its value lies between 100 and 200 [ $\mu m$ ].

Finally, the temperature of the powder bed and feeder affect the final properties of the fabricated parts as well. In particular, it was observed that pre-heating the powder at 300° C mitigates the differences of fatigue resistance between tensile specimens built in different directions: it is possible that the slower cooling rate induced helps reducing the distortions and internal stresses [5].

### Comparer les résultats avec alliage coulé/forgé

Once the porosity problem is sorted out, other matters can be addressed such as productivity and surface roughness. The latter is problematic as the surface finish obtained with SLM is typically of such poor quality that all cracks initiate near the surface for a sample with relative density  $\rho_{rel} > 99\%$  [5]. As said before, it is possible to reduce the surface roughness by mean of a dual scan strategy. However, the only options to obtain significantly better surface finish is currently to machine or polish

the fabricated parts. This is one of the main weak points of SLM.

Post-traitements dont traitements thermiques, sur lesquels on se focalise. Expliquer



## Chapter 3

# Materials and methods

Description expériences et machines

### 3.1 Powder follow-up

#### 3.1.1 Sieving

#### 3.1.2 Grain size and distribution

#### 3.1.3 Composition

### 3.2 Process parameters

The same direct metal printer (DMP) was used to fabricate all specimens throughout this work. It is a *ProX DMP 200* printer, manufactured by *3D Systems* (see figure 3.1). It uses a laser with a theoretical maximal power of 300 [W] and wavelength  $\lambda = 1070$  [nm] [1]. Its actual maximal power is  $P_{max} = 273.6$  [W]. [QUEL EST LE SPOT SIZE?] The maximal envelope capacity of the machine (W x D x H) is 140 x 140 x 125 [mm]. Its typical accuracy is +/- 50 [ $\mu m$ ] for small parts and +/- 0.2% for large parts. It allows for the set-up of a protection atmosphere. However, it does not integrate any heating feature for the build bed.

In this thesis, argon was used as shielding gas. The composition of the gas environment was monitored so as to keep  $p_{O_2} < 500$  [ppm]. Laser compensations were set to take into account the excess energy at the start and end of the scanning vectors (see figure 3.3). These were chosen in accordance with the manufacturer recommendations (figure ??). Values for h and t were respectively set to 100 [ $\mu m$ ] and 30 [ $\mu m$ ]. The other process parameters were varied so as to optimize the properties of the built specimens. Educated guesses were made based on literature and previous works done at the UCL. The parameters used are resumed in table 3.1. Batches were named in the format X200-yyymmdd. The prefix "X200" refers to the DMP used. It is followed by the date of printing (6 digits). Recycled powder was used for every batch except for X200-180222 and X200-180228. The samples fabricated with a contour scanning strategy. are Dimensions of the cubic and cylindrical specimens are noted in accordance with figure 3.4.

All batches were first prepared on *DMP ProX Manufacturing*, a dedicated CAD software. Détails... Insérer images des positions d'échantillons. Aller chercher les ordres de fabrication

Caption des images Batch ... specimens position and order of fabrication

A hexagonal scanning strategy was chosen.. Pourquoi? On nous a pas vraiment demandé notre avis.



FIGURE 3.1: ProX DMP 200 printer (from the user's ProX DMP 200 general instructions document).

Insérer images de trajets du laser.

### 3.3 Heat treatments

The heat treatments were conducted inside a unique oven of the ... model, manufactured by ..., which is able to reach a temperature of 400° C. Samples temperature data was obtained through a thermocouple, welded to the sample surface. The data was displayed and saved every 10 seconds, with a precision of 0.1° C, thanks to a ..., connected to the thermocouple (see Fig. for both devices).

Samples that were subject to a heat treatment were named in a particular format, to ease distinction between them. They receive the name of the batch, followed by "TT-holdingtemperature-holdingtime-specific conditions".

### 3.4 Characterisation

#### 3.4.1 Density

##### Hydrostatic weighing

Multiple methods were considered to estimate the relative density of the fabricated specimens. The first one is hydrostatic weighting (also called hydrodensitometry). It is a direct application of the well-known Archimedes' principle, which can be stated as follows: "When a body is (partially or totally) immersed in a fluid, the upthrust on the body is equal to the weight of fluid displaced." [6]. By weighing each pieces in air and in water - giving respectively values of dry weight  $W_a$  and underwater weight  $W_w$  - one can calculate the apparent density  $\rho_a$  [10]:

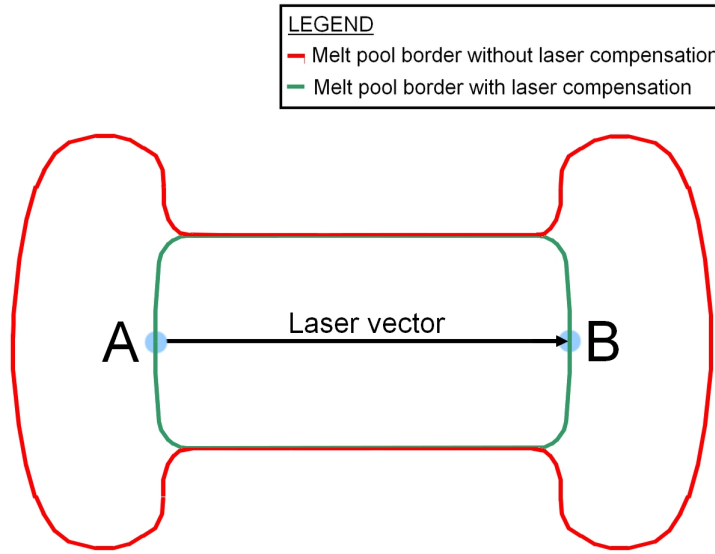


FIGURE 3.2: Melt pool contours with and without laser compensation (exaggeration).

$$\rho_a = \frac{W_a}{W_a - W_w} \cdot \rho_w$$

where  $\rho_w$  is the water density. The apparent relative density  $\rho_{a,rel}$  of the specimens can then be calculated with:

$$\rho_{a,rel} = \frac{\rho_a}{\rho_b}$$

where  $\rho_b = 2.68[\frac{g}{mm^3}]$  is the theoretical bulk density of AlSi10Mg [18]. All weightings were done with a *Sartorius BP121S* analytical balance with precision of 0.1 [mg] [19]. Samples were immersed in demineralised water for more than twelve hours before the measurements to impregnate them. The weightings were also done in demineralised water. Water temperature was measured with a precision glass thermometer to compute  $\rho_w$  as accurately as possible thanks to tabulated values [21].

The technique was employed with "as-built" and polished cubes. This second option reduces the risks of air trapping by the surface roughness, which can distort the results (by overestimating the closed porosities). **A mettre dans la discussion en fait peut-être?** All six faces of the tested cubes were polished with P320 silicon carbide sandpaper sheets and briefly with P1200 ones.

### Relative optical density image analysis

Another method was used to estimate the relative density of the various samples: the relative optical density image analysis (RODIA). For this purpose, the samples underwent the polishing routine detailed in table ?? . Pictures of the polished sections were then taken under the optical microscope.[Infos sur le microscope, grossissement] The pictures were taken with a *Huawei Mate 10 Lite* smart-phone through the

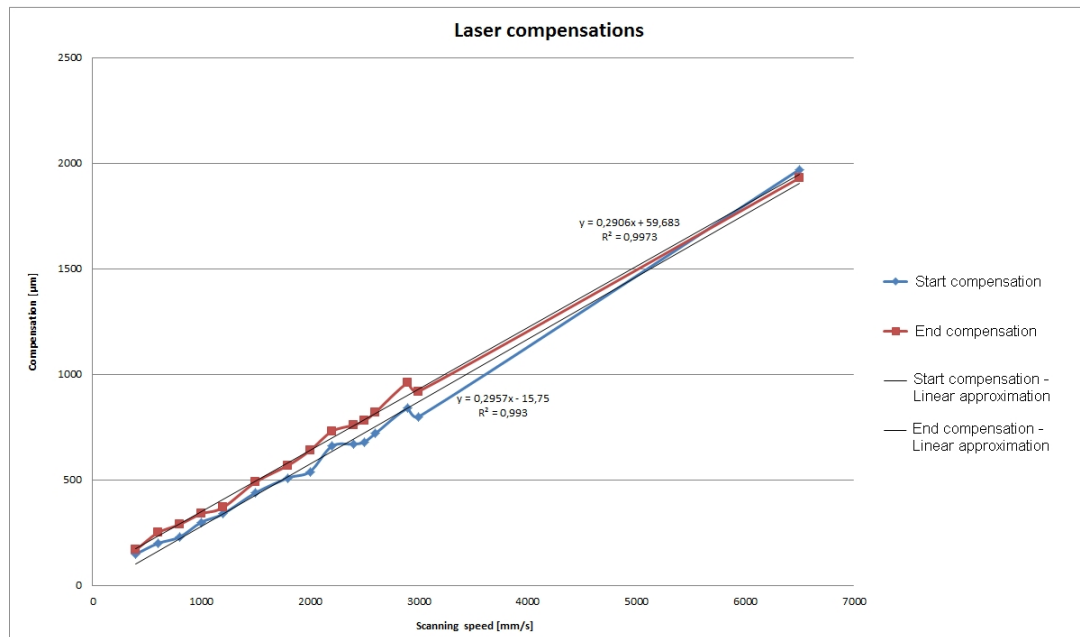


FIGURE 3.3: Laser compensations as a function of the scanning speed (as recommended by the manufacturer).

lens of the microscope. The used camera has a resolution of 16 [MP].

With the help of the *ImageJ* software, the surface of both the porosities and the whole surface could be isolated for each analysed image (see figure 3.5). The surface fraction occupied by porosities could then be obtained as the ratio between the areas of the two (in pixels). If we approximate that the porosities surface fraction is equal to the volumetric one, that method gives an estimation of the relative density  $\rho_{rel}$ .

The images isolations in "foregrounds" and "backgrounds" were done trough manual thresholding based on pixel intensity quantifications. An optimal threshold was sought for porosities isolation so as to include only holes, and as many as possible. [Images avec 2 mauvais seuils et 1 bon]

Difficultés

### 3.4.2 Microscopy

#### Scanning electron microscopy

#### Optical microscopy

Mesures Taille de bords

### 3.4.3 Composition

### 3.4.4 Mechanical properties

#### Hardness test

The hardness o Wolpert Dia-Testor 2RC tester.

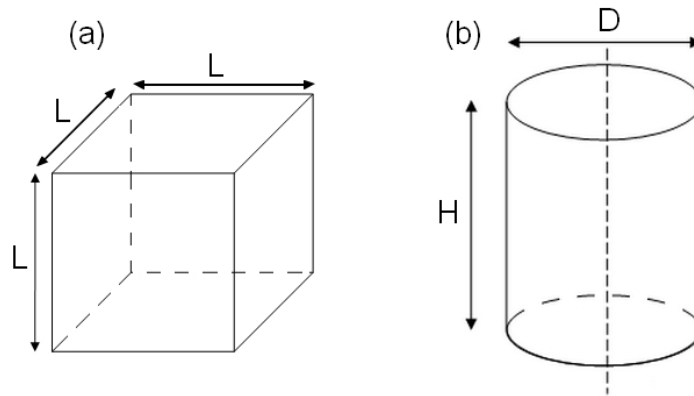


FIGURE 3.4: Dimensions notations for (a) cubic specimens (b) cylindrical specimens

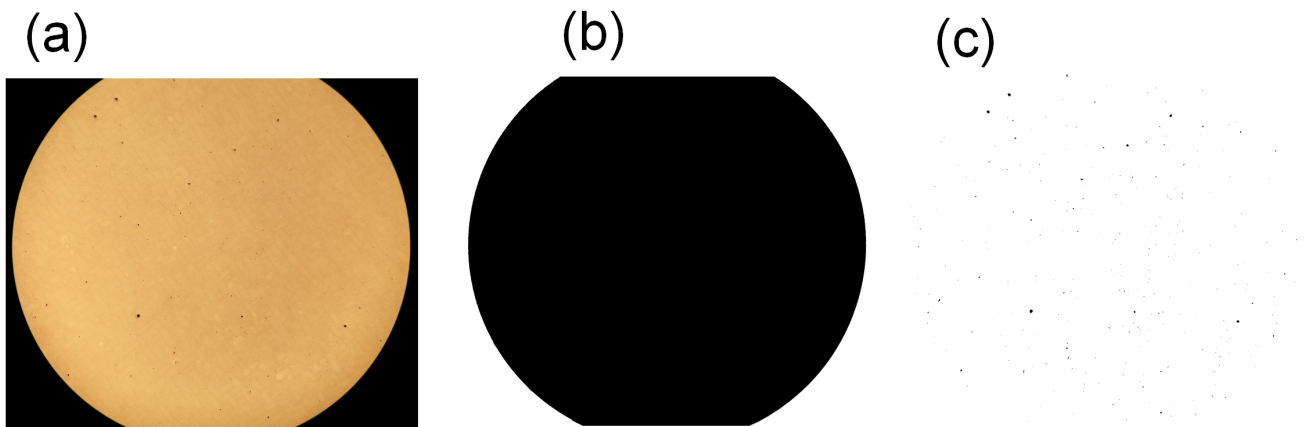


FIGURE 3.5: RODIA procedure for specimen X200-180319-cub 1: (a) Original picture of polished section (b) Whole surface isolation with *ImageJ* (c) Porosities isolation with *ImageJ*.

### Traction test

Batch name	Contour	Type	Dimensions [mm]	Specimen name	$\frac{P}{P_{max}} [-]$	$v_s [\frac{mm}{s}]$
X200-171024	No	Cubic	L=10	1	0.85	900
				2		1000
				3		1059
				4		1500
				5	1	900
				6		1059
				7, 7a, 7b	0.75	1200
				8, 8a, 8b		900
X200-180109	No	Cubic	L=10	7c,...7q (15 spec.) 8c,...8q (15 spec.)	0.75	1200 900
X200-180220	No	Cubic	L=5	TT150-2 TT200-2 TT300-2 TT300-2-plaque TT150-2-real TT200-2-real TT250-2-real TT300-2-real	0.75	1200
X200-180222	No	Cubic	L=10	12 13	0.75	1200
X200-180228	Yes	Cylindrical	D=6, H=2	1 2 3	0.75	1200
X200180313	Yes	Cylindrical	D=6, H=10	1	0.75	1200
				2		
			D=12, H=10	3		
				4		
X200-180319	Yes	Cubic	L=10	cub 1 cub 2 cub 3 cub 4 cub 5	0.75	1200
		Cylindrical	L=5	TT300-1-real		
			D=6, H=10	cyl 1		
				cyl 2		
			D=12, H=10	cyl 3		
				cyl 4		

TABLE 3.1: Process parameters used for the specimens manufacturing

Step	Polishing surface	Abrasive	Grain size	Lubricant type	Rotation speed [rpm]
1	MD-piano 220	Diamond	P220	Water	200-300
2	MD-piano 1200	Diamond	P1200	Water	200-300
3	MD-largo	DP-spray	9 $\mu m$	Alcohol	150
4	DP-DAC	DP-spray	3 $\mu m$	Alcohol	150
5	DP-NAP	DP-spray	1 $\mu m$	Alcohol	150

TABLE 3.2: Polishing routine for Al-Si alloys

## Chapter 4

# Results

Analyses statistiques etc...

### 4.1 Parameters optimisation

### 4.2 Reproducibility

### 4.3 Powder ageing

#### 4.3.1 Grain size and distribution

#### 4.3.2 Composition

Fresh powder

Recycled powder

Date of sampling	Date of last addition of fresh powder	Composition [%wt]			
		Al	Fe	Mg	Si
23/10/2017	07/09/2017	89.2	0.12	0.49	10.2
09/01/2018	07/09/2017	89.3	0.13	0.48	10.1
12/01/2018	07/09/2017	89.4	0.13	0.48	10
21/02/2018	07/09/2017 OU POUDRE NEUVE?	89.1	0.19	0.51	10.3
13/03/2018	22/02/2018	89.1	0.16	0.51	10.1

TABLE 4.1: Composition of recycled AlSi10Mg powder as a function of the date

### 4.4 Heat treatments

### 4.5 Mechanical testing





## **Chapter 5**

# **Discussion**

Que conclure d'après les résultats?

### **5.1 Parameters optimisation**

### **5.2 Reproducibility**

### **5.3 Powder ageing**

#### **5.3.1 Grain size and distribution**

#### **5.3.2 Composition**

### **5.4 Density measures assessments**

### **5.5 Heat treatment optimisation**



## Chapter 6

# Conclusion

They incorporate in a synthetic way the main results and compare them with the initial objectives. Generally, this final chapter also presents prospects for the continuation of the work undertaken.



## Appendix A

# Calculs supplémentaires

**A.1** ...

Impossible

**A.2** ...

... ..



# Bibliography

- [1] 3D Systems Inc, *Direct metal printers: Metal Additive Manufacturing with the ProX<sup>TM</sup> DMP 3D printers*. 2016. URL: [http://sintermedia.gkn.com/blog/the-advantages-of-https://www.3dsystems.com/sites/default/files/2017-01/3D-Systems\\_DMP\\_Tech\\_Specs\\_USEN\\_2017.01.23\\_WEB.pdf](http://sintermedia.gkn.com/blog/the-advantages-of-https://www.3dsystems.com/sites/default/files/2017-01/3D-Systems_DMP_Tech_Specs_USEN_2017.01.23_WEB.pdf) (visited on 13/04/2018).
- [2] Nesma T. Aboulkhair et al. 'On the formation of AlSi10Mg single tracks and layers in selective laser melting: Microstructure and nano-mechanical properties'. In: *Journal of Materials Processing Tech.* 230.Complete (2016), pp. 88–98.
- [3] Nesma T. Aboulkhair et al. 'Reducing porosity in AlSi10Mg parts processed by selective laser melting'. In: *Additive Manufacturing* 1-4 (2014). Inaugural Issue, pp. 77–86. URL: <http://www.sciencedirect.com/science/article/pii/S2214860414000062>.
- [4] Nesma T. Aboulkhair et al. 'Selective laser melting of aluminum alloys'. In: *MRS Bulletin* 42.4 (2017), 311–319.
- [5] Erhard Brandl et al. 'Additive manufactured AlSi10Mg samples using Selective Laser Melting (SLM): Microstructure, high cycle fatigue, and fracture behavior'. In: *Materials & Design* 34 (2012), pp. 159–169. URL: <http://www.sciencedirect.com/science/article/pii/S0261306911005590>.
- [6] John Daintith. *A Dictionary of Physics*. Oxford University Press, 2009. URL: <http://www.oxfordreference.com/view/10.1093/acref/9780199233991.001.0001/acref-9780199233991>.
- [7] Pauline Delroisse et al. 'Effect of strut orientation on the microstructure heterogeneities in AlSi10Mg lattices processed by selective laser melting'. In: *Scripta Materialia* 141 (2017), pp. 32–35. ISSN: 1359-6462.
- [8] Christian Haase et al. 'Exploiting Process-Related Advantages of Selective Laser Melting for the Production of High-Manganese Steel.' In: *Materials* 10(1).56 (2017).
- [9] Simon Hoeges. *Additive manufacturing technologies: 6 Unique Benefits Of Selective Laser Melting*. 2017. URL: <http://sintermedia.gkn.com/blog/the-advantages-of-selective-laser-melting> (visited on 12/04/2018).
- [10] Frank I. Katch. 'Apparent Body Density and Variability during Underwater Weighing'. In: *Research Quarterly. American Association for Health, Physical Education and Recreation* 39.4 (1968), pp. 993–999. URL: <https://shapeamerica.tandfonline.com/doi/abs/10.1080/10671188.1968.10613450>.
- [11] Karolien Kempen et al. 'Microstructural analysis and process optimization for selective laser melting of AlSi10Mg'. In: *Solid Freeform Fabrication Symposium Proceedings* (2011). Conference paper, pp. 484–495. URL: <https://sffsymposium.engr.utexas.edu/Manuscripts/2011/2011-37-Kempen.pdf>.

- [12] K.-H. Leitz et al. 'Multi-physical simulation of selective laser melting'. In: *Metal Powder Report* 72.5 (2017), pp. 331–338. URL: <http://www.sciencedirect.com/science/article/pii/S0026065716300200>.
- [13] Rene Lippert and Roland Lachmayer. 'A Design Method for SLM-Parts Using Internal Structures in an Extended Design Space'. In: (Sept. 2018), pp. 14–23.
- [14] Bochuan Liu et al. 'Investigaztion the effect of particle size distribution on processing parameters optimisation in selective laser melting process'. In: (Jan. 2011). Conference paper, pp. 227–238.
- [15] Anne I. Mertens, Jocelyn Delahaye and Jacqueline Lecomte-Beckers. 'Fusion-Based Additive Manufacturing for Processing Aluminum Alloys: State-of-the-Art and Challenges'. In: *Advanced Engineering Materials* 19.8 (2017), p. 1700003. URL: <https://onlinelibrary.wiley.com/doi/abs/10.1002/adem.201700003>.
- [16] K.G. Prashanth, S. Scudino and J. Eckert. 'Defining the tensile properties of Al-12Si parts produced by selective laser melting'. In: *Acta Materialia* 126 (2017), pp. 25–35. URL: <http://www.sciencedirect.com/science/article/pii/S135964541630982X>.
- [17] Noriko Read et al. 'Selective laser melting of AlSi10Mg alloy: Process optimisation and mechanical properties development'. In: *Materials & Design* (1980-2015) 65 (2015), pp. 417–424. URL: <http://www.sciencedirect.com/science/article/pii/S0261306914007468>.
- [18] Renishaw plc, *AlSi10Mg-0403 powder for additive manufacturing data sheet*. 2015. URL: [file:///E:/Downloads/H-5800-1061-01-A\\_AlSi10Mg-0403\\_400\\_W\\_material\\_data\\_sheet.pdf](file:///E:/Downloads/H-5800-1061-01-A_AlSi10Mg-0403_400_W_material_data_sheet.pdf) (visited on 15/04/2018).
- [19] Sartorius AG, *Sartorius BP121S Installation And Operating Instructions Manual*. 2000. URL: <https://www.manualslib.com/products/Sartorius-Bp121s-3748053.html> (visited on 15/04/2018).
- [20] Ming Tang, P. Chris Pistorius and Jack L. Beuth. 'Prediction of lack-of-fusion porosity for powder bed fusion'. In: *Additive Manufacturing* 14 (2017), pp. 39–48. URL: <http://www.sciencedirect.com/science/article/pii/S2214860416300471>.
- [21] Robert C Weast. *CRC Handbook of Chemistry and Physics 53rd Edition*. CRC Press, 1973. URL: [http://jupiter.plymouth.edu/~jsduncan/courses/2012\\_Spring/Techniques/Exams/DensityOfWater-vs-Temp.pdf](http://jupiter.plymouth.edu/~jsduncan/courses/2012_Spring/Techniques/Exams/DensityOfWater-vs-Temp.pdf).
- [22] Christian Weingarten et al. 'Formation and reduction of hydrogen porosity during selective laser melting of AlSi10Mg'. In: *Journal of Materials Processing Technology* 221 (2015), pp. 112–120. URL: <http://www.sciencedirect.com/science/article/pii/S0924013615000564>.
- [23] Chor Yen Yap et al. 'Review of selective laser melting: Materials and applications'. In: 2 (Dec. 2015), p. 041101.